Kashani, M. M., Lowes, L. N., Crewe, A. J., & Alexander, N. A. (2015). Phenomenological hysteretic model for corroded reinforcing bars including inelastic buckling and low-cycle fatigue degradation. *Computers and Structures*, *156*, 58–71. https://doi.org/10.1016/j.compstruc.2015.04.005

Phenomenological hysteretic model for corroded reinforcing bars including inelastic buckling and low-cycle fatigue degradation

Mohammad M. Kashani[1], Laura N. Lowes[2], Adam J. Crewe[3], Nicholas A. Alexander[4]

Abstract

A new phenomenological hysteretic model for reinforcing bars with and without corrosion damage is presented. The model simulates buckling of reinforcement, deterioration in post-buckling compressive strength due to strain history and the impact of low-cycle fatigue on tension response. The model, for uncorroded reinforcing bars, is calibrated using data from numerical simulations and corrosion damage parameters are calibrated using experimental data. The model is evaluated using a comprehensive experimental data set, and the results show that the model is in a good agreement with the data.

Keywords: Reinforcing steel; Corrosion; Inelastic buckling; Hysteretic model; Cyclic behaviour; Constitutive modelling; Low-cycle fatigue.

1 Introduction

Nonlinear analysis of reinforced concrete (RC) structures subject to seismic loading often employs fibre-type section models to simulate the flexural response of beams, columns and walls. These fibre-type section models are typically used within a plastic hinge or a lumped- or distributed-plasticity beam-column elements [1,2]. Examples include implementations in OpenSees, SeismoStruct and SAP2000 [3,4,5]. Using a fibre-type section model, the member cross section is decomposed into a number of steel and concrete fibres. The material nonlinearity is represented through uniaxial constitutive models for steel and confined and unconfined concrete. Therefore, the accuracy of the model is highly dependent on the accuracy of the uniaxial constitutive models.

[1]Lecturer, University of Bristol, Dept. of Civil Engineering University of Bristol, Bristol, BS8 1TR, United Kingdom (corresponding author), E-mail: mehdi.kashani@bristol.ac.uk
[2]Associate Professor, University of Washington, Dept. of Civil and Environmental Engineering University of Washington, Seattle, WA 98195-2700, United States of America
[3]Senior Lecturer, University of Bristol, Dept. of Civil Engineering University of Bristol, Bristol, BS8 1TR, United Kingdom
[4]Senior Lecturer, University of Bristol, Dept. of Civil Engineering University of Bristol, Bristol, BS8 1TR, United Kingdom

Previous research shows that fibre-type section models and lumped or distribution plasticity element can provide highly accurate simulation of the stiffness, strength and cyclic response of RC members through moderate deformation demands [6,7]. However, few studies have addressed simulation of response to loss of lateral and, ultimately, axial load carrying capacity; and few studies have demonstrate accurate simulation of drift capacity (i.e. the drift at onset of significant lateral strength loss) [8]. For RC members responding in flexure, strength loss typically results from buckling of longitudinal reinforcement, fracture of longitudinal reinforcing due to low-cycle high-amplitude fatigue and/or crushing of core confined concrete. The research presented here focusses on simulating the behaviour of reinforcing steel with the objective of enabling accurate simulation of component failure.

In previous decades, a number of researchers have studied the cyclic behaviour of reinforcing steel with and without buckling [9-23]. They have tried to address simulation of uncorroded reinforcement; however, there are many critical structures that are located in regions of high seismicity and that are exposed to corrosive environments. Recent experimental studies of the cyclic behaviour of RC elements with corroded reinforcement show that corrosion has a significant impact on the response of these structures [24,25]. The experimental results showed that corrosion will change the failure mode of flexural RC components.

In some cases severe buckling were observed due to the combined effects of non-uniform pitting corrosion along the longitudinal reinforcement and corrosion of horizontal ties. Corrosion reduces the stiffness of horizontal ties that are very important elements to prevent the buckling of longitudinal bars. Once corroded bars buckle under cyclic loading, they fracture much faster at lower drift demands. This is due to the combined effect of buckling and non-uniform pitting corrosion that results in a significant reduction in low-cycle fatigue life of corroded RC elements. Accordingly, Kashani *et al.* [23,26-28] conducted a comprehensive experimental and computational study on the inelastic behaviour of corroded reinforcing bars, including the impact of corrosion pattern on inelastic buckling and degradation due to low-cycle fatigue.

Moreover, Kashani *et al.*[23, 28] explored that the inelastic buckling of reinforcing bars results in a severe pinching effect on the cyclic stress-strain response of reinforcing bars. This phenomenon is due to the effect of geometrical nonlinearity. This behaviour is not included in any of the previous models [9-11, 13, 19]. Therefore, one of the objectives of the current paper is to address this important issue.

Here a new phenomenological hysteretic model is developed that significantly improves the inelastic buckling simulation of reinforcing steel with and without corrosion damage. The aims of this paper are:

- To describe this new model that accounts for the combined effect of inelastic buckling and low-cycle fatigue.
- To demonstrate that this new model accounts for the influence of corrosion damage on inelastic buckling and low-cycle high-amplitude fatigue degradation of reinforcing bars.
- To calibrate and validate this model against an extensive experimental and computational data set.

The proposed model combines the material nonlinearity and geometrical nonlinearity due to buckling with low-cycle fatigue degradation in to a single material model. This model is currently the most advanced uniaxial material model which is purposely developed for reinforcing bars with and without corrosion damage. Finally, this advanced uniaxial material model has been implemented to the OpenSees [3] to enable the earthquake engineering community to use it in the nonlinear seismic analysis of uncorroded and corroded RC structures.

2 Modelling the nonlinear response of reinforcing bars with the effect of buckling and low-cycle high amplitude fatigue without corrosion damage

Kashani *et al*. [28] conducted a parametric study of the nonlinear cyclic behaviour of reinforcing bars with and without corrosion damage. The results of computational modelling showed that increasing the L/D ratio beyond 8 (L is the length and D is the diameter of reinforcing bars used in either experiment or finite element model) in reinforcing bars with yield strength between 400MPa and 500MPa results in a complex pinching effect in the hysteretic cycles. This is the influence of geometrical nonlinearity on the cyclic response. Other researchers have also come up with the same conclusion based on the experimental results [21-23]. This shows a stable pattern in cyclic behaviour of reinforcing bars with the effect of buckling.

Kashani *et al*. [28] have made a comparison between the existing analytical models and the computational results. They have demonstrated that the pinching effect due to the geometrical

nonlinearity is not included in the existing analytical models (e.g. *ReinforcingSteel* model in OpenSees). The pinching effect in hysteretic cycles of longitudinal reinforcement has a significant influence on the cyclic degradation of RC components subject to seismic loading. Therefore, it needs to be considered in the material model of reinforcement in nonlinear analysis of RC structures under cyclic loading. Accordingly, a set of cyclic rules have been developed in this paper to capture this complex phenomenon.

2.1 Overview of the proposed model

The proposed model consists of seven main states. (1) tension envelope (TE), (2) compression envelope (CE), (3) unload-reload response for compression to tension (URCT), (4) unload-reload response for tension to compression (URTC), (5) incomplete unload-reload cycles (IURC), (6) degradation in buckling strength due to cyclic loading (BUCKDEG), (7) degradation in tension strength due to low-cycle fatigue / cyclic loading (FATDEG). A diagram of the four main states of the proposed model is shown in Fig. 1. The incomplete unload-reload state and degradation states are not included as they are essentially just modifications of the four basic states and full details of these states are provided later in the paper.

Table 1 summarises the analytical equations and calibration methods used for each state. A mixture of experimental and numerical data have been used to calibrate the model parameters.

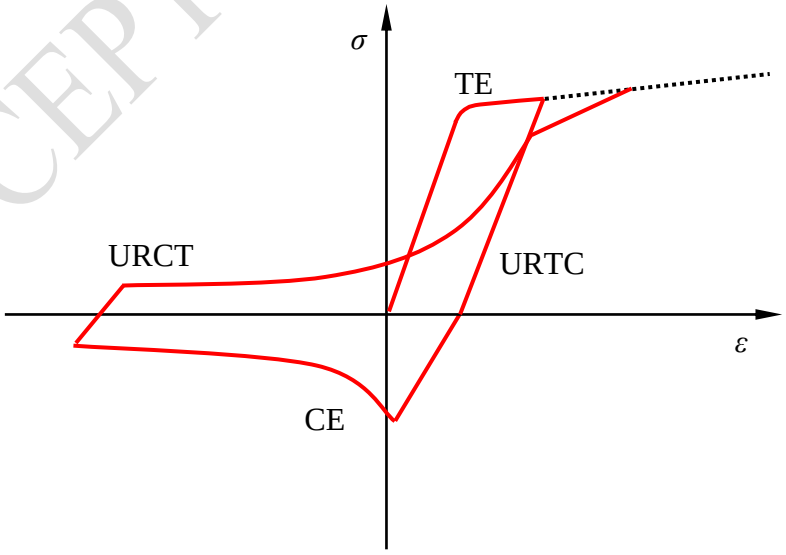

Fig. 1 Proposed phenomenological hysteretic model

To calibrate the model parameters in the proposed model a comprehensive set of experimental and numerical dataset reported by Kashani *et al*. [23, 26, 28] is used. The material data for both monotonic bucking and cyclic loading are available in [23, 26]. The numerical data used to calibrate the post-buckling behaviour is available in [28].

Table 1 Summary of model states and calibration methods

State	Type of data used in calibration	Equation number in this paper
TE	Experimental	Eq. (1)
CE	Experimental and numerical	Eqs. (2) to (6)
URCT	Experimental	Eqs. (10) to (16)
URTC	Experimental and numerical	Eqs. (7) to (9)
IURC	Experimental	Eq. (17)
BUCKDEG	Numerical	Eq. (7)
FATDEG	Experimental	Eq. (24)

2.2 Modelling tension response (state TE)

Several models available in the literature define the tension envelope for reinforcing steel [13-16,29]. The model proposed by Balan *et al*. [15] employs a continuous function that provides a smooth transition from linear elastic to strain hardening region (Fig. 2). This will improve the numerical stability of nonlinear finite element analyses. Therefore, this model is use to define the tension envelope (Eq. (1)).

$$\sigma = \sigma_y \frac{(1-\mu)}{2}\left[1+\frac{(1+\mu)}{(1-\mu)}\frac{\varepsilon}{\varepsilon_y}-\sqrt{\left(\frac{\varepsilon}{\varepsilon_y}\right)^2+\delta}\right] \quad (1)$$

where $\mu = E_h / E_s$ is the hardening ratio with E_s and E_h equal to the elastic modulus and hardening modulus for the steel, σ_y is the yield stress, ε is the current strain, ε_y is the yield strain and δ is a shape parameter. Eq. (1) represents a hyperbola with two asymptotes, one with slope E_s and one with slope E_h. The shape parameter, δ, defines the curvature radius of the transition between linear elastic to hardening region of the curve. Further details of this model are available in [15].

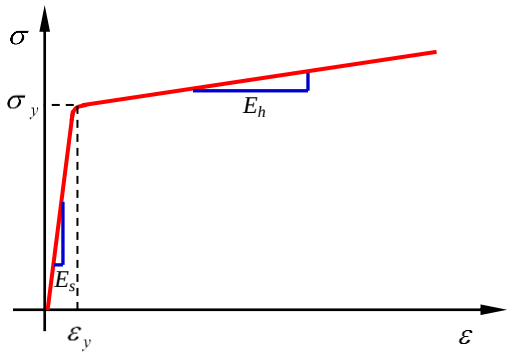

Fig. 2 Balan *et al* [15] Tension envelope model

2.3 Modelling compression response (state CE)

Mau and El-Mabsout [30] developed a special beam-column element for nonlinear finite element analysis of the inelastic buckling of reinforcing bars. This model can correctly simulate the inelastic buckling of a single reinforcement bar but it is computationally expensive for use in nonlinear analysis of RC structures. Monti and Nuti [9] developed an analytical model based on experimental tests on reinforcing bars. This model is simple and suitable for incorporation into the computational section analysis that is found within a nonlinear analysis of RC structures and it uses a fibre-based section decomposition method.

However, this model doesn't account for cyclic degradation and the impact of buckling on pinching response of reinforcing bars. Moreover, this model is only valid for buckling simulation of reinforcing bars with $L/D < 8$. Dhakal and Maekawa [18] conducted a nonlinear finite element analysis on single reinforcing bars with different L/D ratios using a fibre-based technique. They found that the post-yield buckling behaviour of reinforcing bars is governed by the combined influence of L/D ratio and the yield stress σ_y of the reinforcement. Considering this assumption, they have developed a trilinear analytical model to represent the post-yield buckling behaviour of reinforcing bars. In this model, the compression response of reinforcement is defined as a function of a single compound variable called the non-dimensional slenderness ratio λ_p as defined in Eq. (2) below:

$$\lambda_p = \sqrt{\frac{\sigma_y}{100}}\frac{L}{D} \tag{2}$$

where σ_y has units of MPa.

The yield stress of the most commonly used reinforcing bars in construction of RC structures around the world ranges between 400 MPa to 500 MPa. The experimental results and computational modelling of reinforcing bars for these bars showed that buckling is not critical for the groups of bars with $L/D < 6$. Therefore, they can be treated in a similar manner to their tension behaviour.

The group of bars with $6 \le L/D < 8$ buckle under compression, however, given the buckling length is very small the influence of buckling doesn't result in the softening type behaviour post yield. The behaviour of this group of bars in compression can be treated as elastic perfectly plastic model.

However, once the *L/D* ratio exceeds 8 (*L/D* > 8) the inelastic buckling results in a post-buckling softening response. Accordingly, the proposed model in this paper significantly improves the simulation of stress-strain response of reinforcing bars with *L/D* ≥ 8. The main contributions of the current paper are simulation of the buckling response of reinforcing bars with $8 \le L/D \le 30$, accounting for cyclic and fatigue degradation, accounting for degradation of buckling strength under cyclic loading and influence of buckling on pinching response of stress-strain curve. The parameters defining the post-yield buckling curve are a function of the λ_p. Therefore, the methodology proposed by Dhakal-Maekawa [20] can be used to calculate the buckling length considering the influence of the stiffness of horizontal tie on buckling of vertical reinforcement within RC elements.

2.4 Inelastic buckling response (in state CE)

The model proposed in this paper employs an exponential function to describe the post-yield bucking response of reinforcing bars as shown in Fig. 3. This approach has been used previously by others to model the inelastic buckling behaviour of concentric steel bracing [31, 32]; here the post-buckling curve is defined in Eq. (3):

$$\sigma = \begin{cases} E_s\,\varepsilon & : \varepsilon \le \varepsilon_y \\ \sigma^* + \left(\sigma_y - \sigma^*\right) \exp\left(-\left(\rho_1 + \rho_2\sqrt{\varepsilon_p}\right)\left(\varepsilon_p\right)\right) & : \varepsilon > \varepsilon_y \end{cases} \quad \text{for} \quad 8 \le L/D \le 30 \qquad (3)$$

where ρ_1 is the initial tangent of the post-buckling response curve, ρ_2 is the rate of change of the tangent, ε is the current strain, $\varepsilon_p = \varepsilon - \varepsilon_y$ is the plastic strain, σ^* is the asymptotic lower stress limit of the post-buckling curve, and all other variables are as previously defined. The

parameters ρ_1, ρ_2 and σ^* are defined by the yield strength and geometrical slenderness ratio of the reinforcing steel, as discussed in the following section.

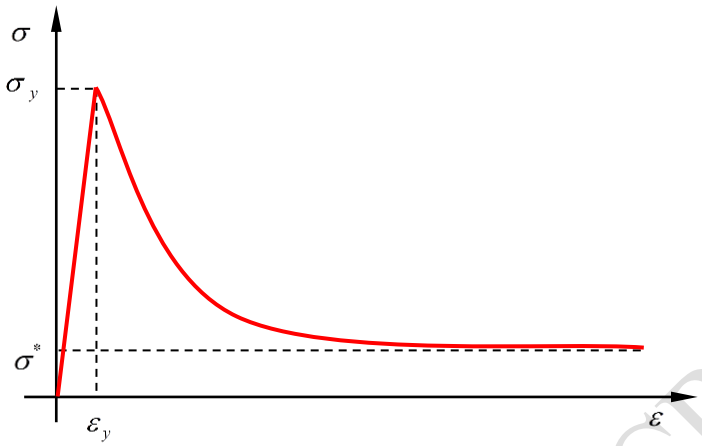

Fig. 3 Proposed analytical model for post-yield buckling envelope

2.5 Calibration of the model parameters for post-yield buckling (in state CE)

Nonlinear finite element analysis of isolated reinforcing bars subjected to monotonic compressive displacement histories were used to develop models defining the parameters ρ_1, ρ_2 and σ^* as a function of reinforcement yield strength and geometric slenderness ratio (L/D). Previous research by the authors of this paper and others validates this approach to model calibration [18,20,21,28,30]. For the current study, the OpenSees software platform and the co-rotational force-based fibre-type beam-column element were used; Kashani *et al.* [28] provides a detailed discussion of the model.

Approximately fifty analyses were conducted for reinforcing bars with L/D varying from 8 to 30 and yield strengths ranging from 100 MPa to 600 MPa. The analysis data related to the post-buckling branch of each case exported to MATLAB [33]. Using the CFT (curve fitting toolbox) available in MATLAB, the Eq. (3) fitted to each post-buckling response analysis curve. Using this approach the parameters ρ_1, ρ_2 and σ^* in Eq. (3) were optimised to provide the best fit to the simulated post-buckling response of the bar. The optimised model parameters (ρ_1, ρ_2 and σ^*) for each analysis case from the curve fitting procedure were stored in a vector. Finally, regression analysis was used to determine the correlation between the model parameters and bar yield strength and geometrical slenderness ratio (λ_p).

Ultimately, it was found that *i*) ρ_1 is strongly, positively correlated with λ_p,, *ii*) ρ_2 is strongly negatively correlated with λ_p, *iii*) σ^* is minimally correlated with λ_p, and *iv*) σ^* has a strong

positive correlation with σ_y /*L/D*. Fig. 4 (a-c) shows the model parameters determined from the simulation data as well as the models resulting from the regression analyses and correlation coefficients. The details of simulation and discussion of results shown in Fig. 4 are available in [28].

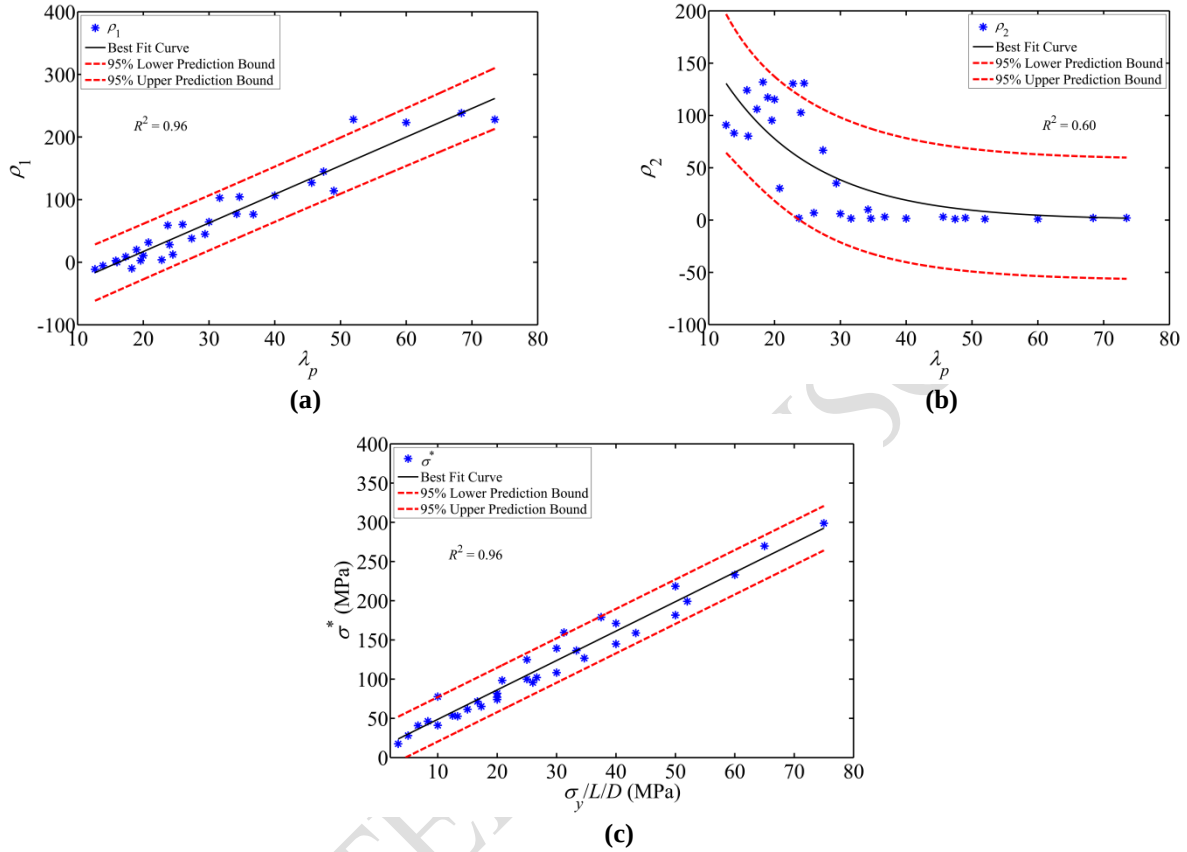

Fig. 4 Calibration of the post-buckling model parameters: a) ρ_1 b) ρ_2 c) σ^*

The regression analyses resulted in the following equations defining the buckling model parameters:

$$\rho_1(\lambda_p) = 4.572\,\lambda_p - 74.43 \tag{4}$$

$$\rho_2(\lambda_p) = 318.40\,\exp(-0.071\lambda_p) \tag{5}$$

$$\sigma^* = 3.75\,\frac{\sigma_y}{\frac{L}{D}} \tag{6}$$

2.5.1 Experimental validation of the buckling model (in state CE)

Data from numerical simulations were used to calibrate the model parameters. The numerical simulation has been done using OpenSees. In the simulation a nonlinear fibre beam-column element used to model the reinforcing bars. Further details are available in [28].

The proposed buckling model was then validated using data from the experimental tests of isolated reinforcing bars reported in [26]. Fig. 5 (a-d) shows a comparison between the calibrated model, numerical simulation data and experimental data.

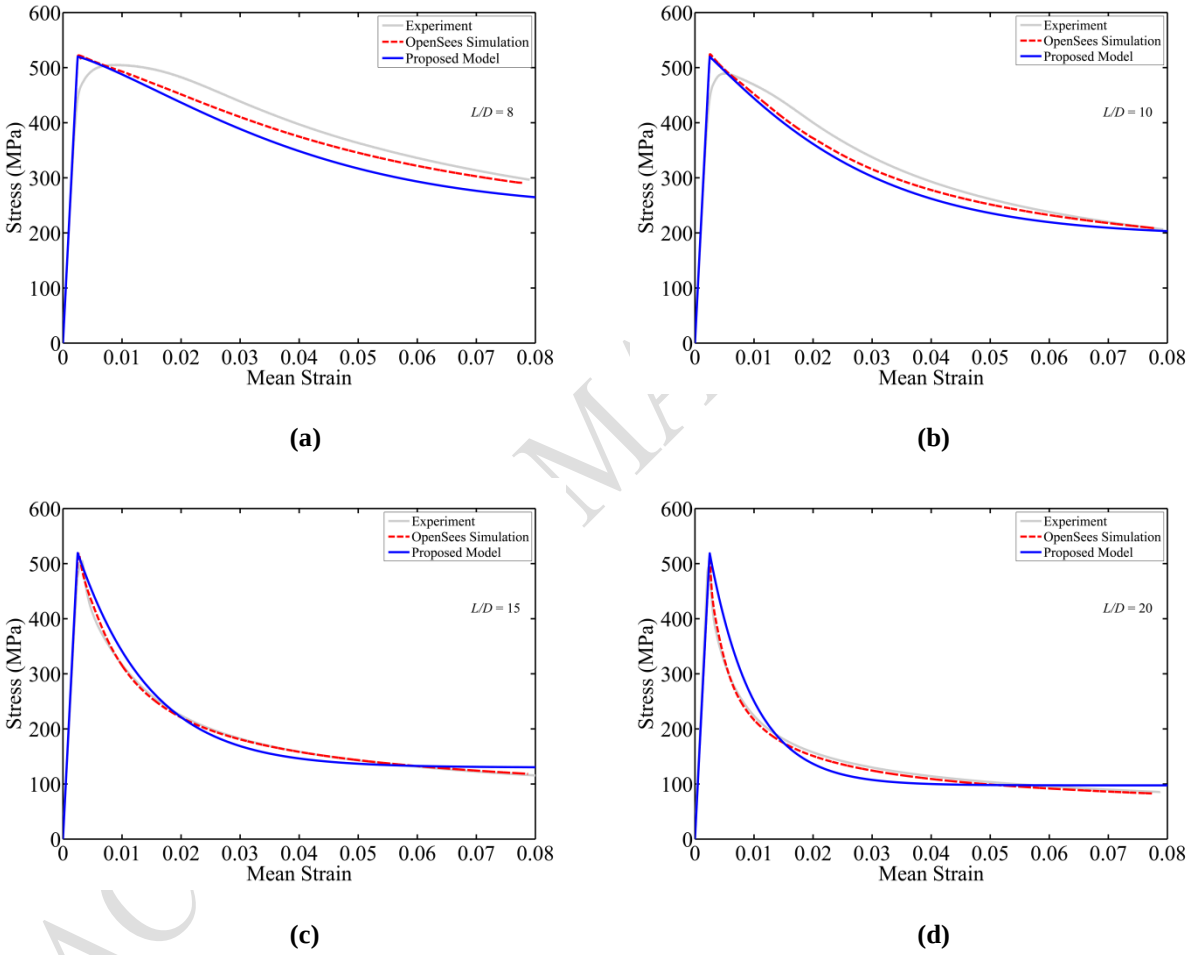

Fig. 5 Verification of the proposed analytical model: a) *L/D* = 8 b) *L/D* = 10 c) *L/D* = 15 d) *L/D* = 20

It should be noted that the experimental graphs shown in Fig. 5 were not included in the calibration process. Therefore, it is evident from Fig. 5 that the proposed model can accurately predict the post-yield buckling response of reinforcing bars.

2.6 Modelling the cyclic response (states BUCKDEG and URTC)

2.6.1 Degradation of buckling strength and unloading-reloading stiffness from tension to compression under cyclic loading

Previous research shows that under cyclic loading the buckling strength and unloading-reloading response from tension to compression of reinforcing bars is a function of the strain history. Experimental data show that the buckling strength of bars is a function of the plastic tension strain history as well as the slenderness ratio [22].

For the current study, the results of nonlinear finite element analyses of bare reinforcing bars were used to develop data relating strain history and degradation of the buckling strength and unloading–reloading stiffness. A series of analyses were conducted for reinforcing bars with varying λ_p (Eq. (1)) and varying strain history. Kashani *et al.* [28] describes the model and the analyses. In these analyses, the bar has been pulled in tension and pushed back to compression at various tension strains to find the influence of tension strain on buckling strength. Fig. 6 shows an example simulation result for a reinforcing bar with L/D = 20 and σ_y = 500.

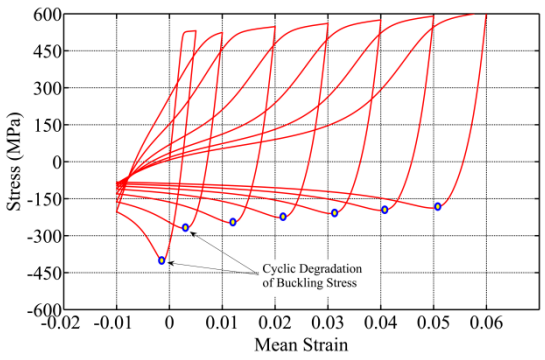

Fig. 6 Numerical simulation of cyclic degradation of buckling stress (L/D = 20)

Fig 7 (a) shows model parameters defining the buckling strength and unload-reload stiffness. Simulation data and regression analysis were used to develop a model defining the degradation in buckling strength as a function of plastic strain demand in tension, ε_p, and the non-dimensional slenderness ratio, λ_p. Fig. 7 (b) shows buckling strength reduction under cyclic loading versus ε_p λ_p as determined from numerical simulation (blue data points) as well as the model resulting from regression analysis of the data (black line):

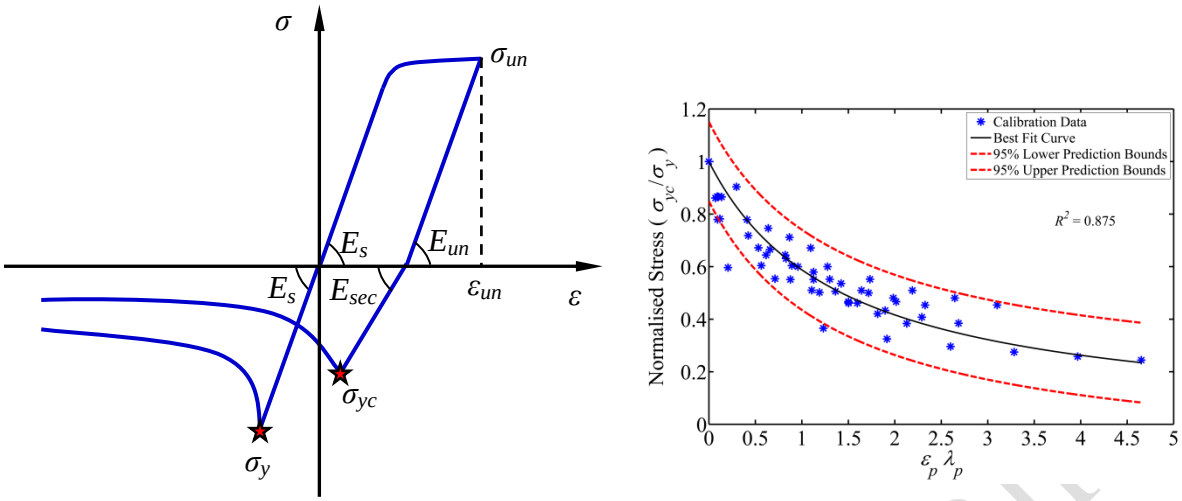

(a) **(b)**

Fig. 7 Modelling tension unloading and compression reloading branch: a) schematic view of model and b) calibration of cyclic degradation of buckling stress

$$\frac{\sigma_{yc}}{\sigma_y} = \frac{1}{1+0.7\,\varepsilon_p\,\lambda_p} \qquad \sigma_{yc} \geq 0.25\sigma_y \tag{7}$$

where σ_{yc} is the buckling stress under cyclic loading and ε_p is the plastic strain in tension defined as $\varepsilon_p = \varepsilon_{un} - \varepsilon_y$ with ε_{un} equal to the maximum historic tension strain.

Dodd and Restrepo [14] use data from bare bar tests to develop an empirical equation defining unloading stiffness, from tension to compression, as a function of plastic tension strain. Despite the results of these previous research efforts, the impact of cyclic loading on buckling strength and unload-reload stiffness has not been incorporated in constitutive models for reinforcing steel.

The empirical equation proposed by Dodd and Restrepo [14] (Eq. (8)) is used to define the unloading stiffness, E_{un}. The data from numerical simulations of bare bars were used to define the reloading stiffness, E_{sec}, for reloading to compression as defined in Eq. (8) and (9).

$$\frac{E_{un}}{E_s} = 0.82 + \frac{1}{5.55+1000\,\varepsilon_p} \tag{8}$$

$$\frac{E_{\sec}}{E_s} = \frac{1}{1+\left(\dfrac{\varepsilon_p}{0.005}\right)^{0.5}} \qquad E_{\sec} \geq 0.2\,E_s \tag{9}$$

2.6.2 Cyclic stiffness degradation of compression unloading and tension reloading (state URCT)

[23, 28] show that for reinforcing bars with $L/D \geq 8$, the unloading-reloading from compression to tension is significantly affected with increasing strain demand. At small strain demands, the unloading-reloading branch is convex in shape. However as strain demand increases, the unloading-reloading response curve becomes concave and pinched. To capture this behaviour in the model, different equations are used for unloading at small and large strain demands. Similar behaviour was observed by other researchers [21,22].

In the proposed model two types of curves are introduced at low and high strain demands. If unloading occurs at low strain demand ($\varepsilon \leq 9\varepsilon_y$) a trilinear curve that is shown in Fig. 8 is used.

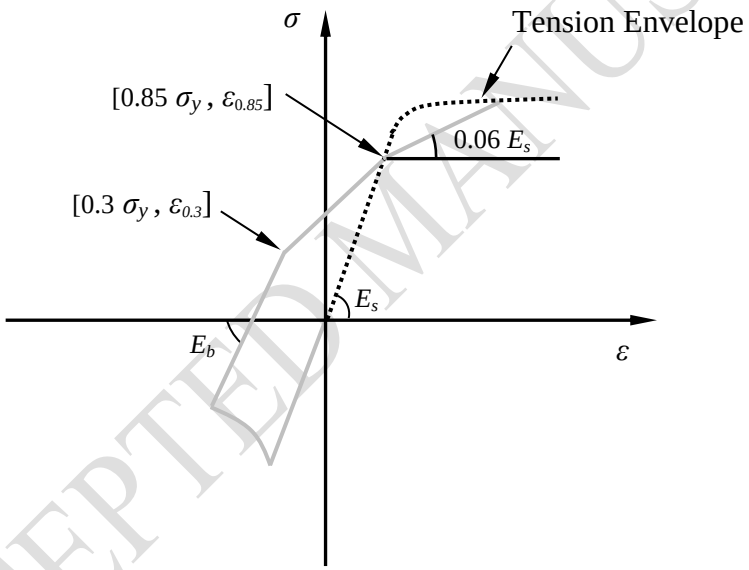

Fig. 8 Multi-linear curves to model compression unloading branch at small strain demand ($\varepsilon \leq 9\varepsilon_y$)

The concave shape of the compression unloading branch at large strain demand ($\varepsilon > 9\varepsilon_y$) is modelled using linear-hyperbolic curves as shown in Fig. 9. The initial unloading stiffness E_b is defined in Eq. (10).

$$\frac{E_b}{E_s} = \left(\frac{\sigma_{\min}}{\sigma_{t\min}} \right)^{1.5} \tag{10}$$

where, σ_{min} is the minimum compressive stress at unloading and σ_{tmin} is the stress in tension envelope corresponding to the strain at σ_{min} (Fig. 9 (a)).

The hyperbolic curve between the point at 0.15 σ_y and 0.85 σ_y (Fig. 9 (b)) is defined in the following Eq. (11) to (16).

$$\sigma_h = \frac{\varepsilon_h}{\eta_1 + \eta_2\,\varepsilon_h} \tag{11}$$

$$\eta_1 = \begin{cases} \dfrac{1}{0.03\,E_s} & : \quad \lambda_p \le 45 \\ \dfrac{1}{0.015\,E_s} & : \quad \lambda_p > 45 \end{cases} \tag{12}$$

$$\eta_2 = \frac{1}{0.15\,\sigma_y - 0.85\sigma_y} - \frac{\eta_1}{\varepsilon_{0.15} - \varepsilon_{0.85}} \tag{13}$$

$$\varepsilon_{0.85} = \varepsilon_{un} - \frac{\sigma_{un} - 0.85\sigma_y}{E_{un}} \tag{14}$$

$$\sigma = \sigma_h + 0.15\,\sigma_y \tag{15}$$

$$\varepsilon = \varepsilon_h + \varepsilon_{0.15} \tag{16}$$

All of the above variables are defined in Fig. 9.

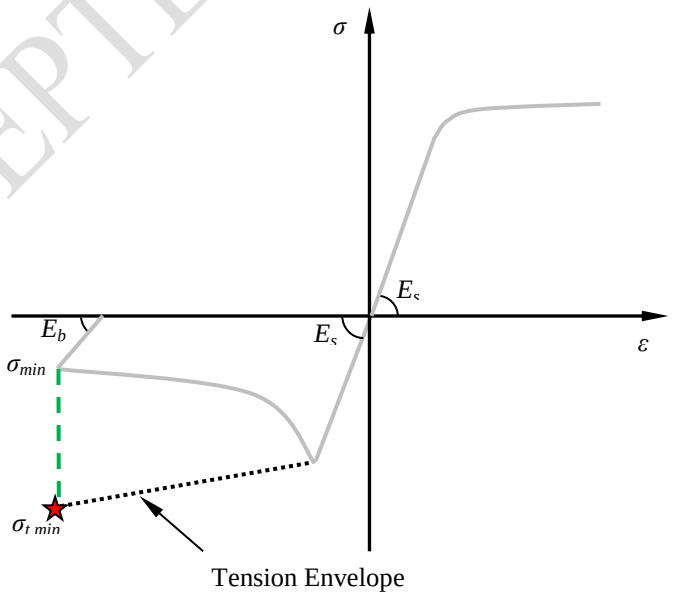

(a)

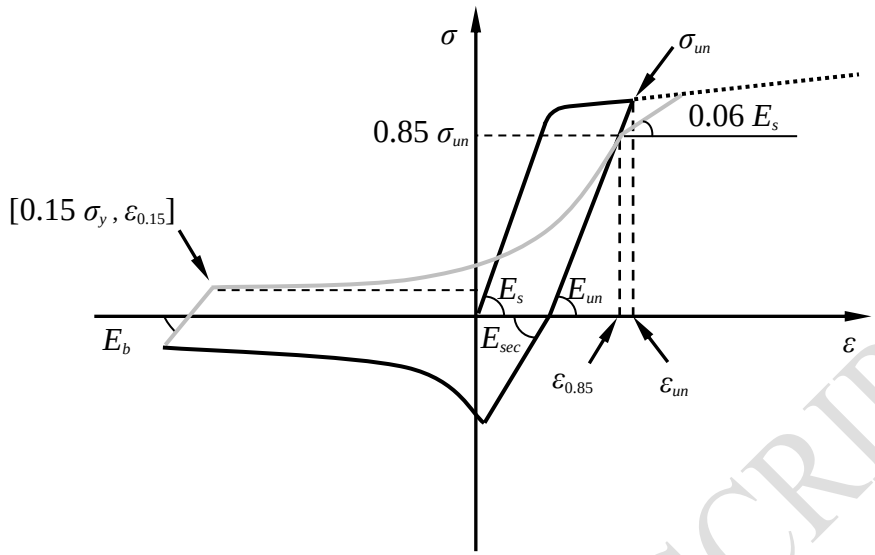

(b)

Fig. 9 Linear-hyperbolic curves to model compression unloading branch at large strain demand ($\varepsilon > 9\varepsilon_y$): (a) definition of the initial stiffness E_b and (b) unloading-reloading rule

2.6.3 Unloading rules from URCT and URTC states (state IURC)

To enable response simulation for general displacement histories, it is necessary to define behaviour for the case of a strain reversal that occurs on an unload-reload path prior to reaching the compression or tension envelope. Here the strain reversal is defined by Eq. (17).

$$\left(\varepsilon_{i-1}-\varepsilon_{i-2}\right)\left(\varepsilon_i-\varepsilon_{i-1}\right)<0 \tag{17}$$

where ε_i is the total strain at the current time step, i, and ε_{i-1} and ε_{i-2} are the total strains at previous time steps. If the bar experiences a strain reversal prior to buckling, the unload-reload path is linear with a stiffness equal to the E_{un} of the previous tension unloading path until it intersects with the tension envelop (Fig. 10(a)). If the bar experiences a strain reversal while unloading from compression to tension, the unloading path is linear with stiffness equal to the E_{sec}, until it intersects with the post-buckling envelope (Fig. 10 (b)).

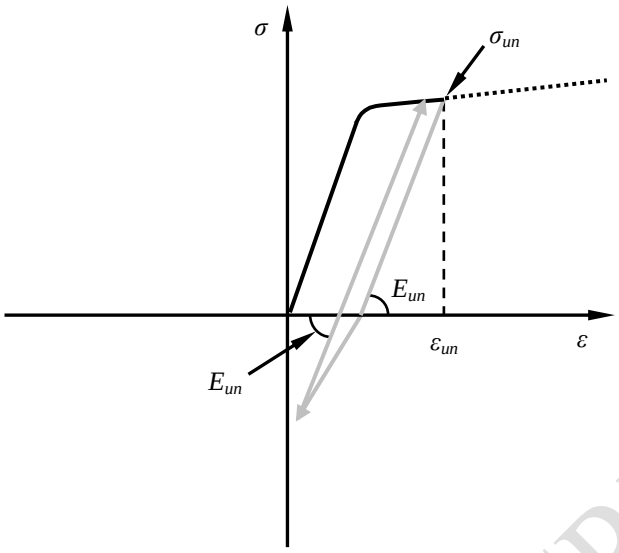

(a)

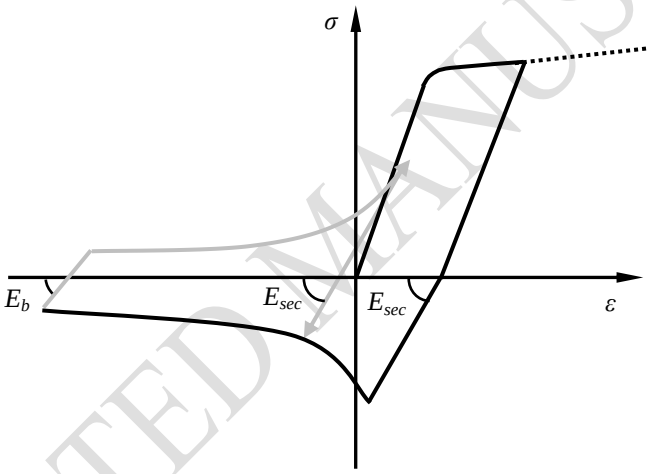

(b)

Fig. 10 Unloading rules from incomplete cycles: a) pre-buckling state b) post-buckling state

2.6.4 Modelling low-cycle fatigue degradation (state FATDEG)

The experimental data showed that the combined effects of pitting corrosion and low-cycle high-amplitude fatigue result in degradation of the tension strength [23]. Strength degradation for uncorroded reinforcing bars due to low-cycle fatigue has been investigated experimentally by other researchers [34-37]. The Coffin-Manson [38] fatigue-life model (Eq. (18)) is widely used [36-39] to predict the bar fracture strain in tension.

$$\varepsilon_p = \Theta_f \left(2N_f\right)^{-\alpha} \tag{18}$$

where ε_p is the plastic strain amplitude ($\varepsilon_p = \varepsilon_a - \varepsilon_y$ where, ε_a is the total strain amplitude), $2N_f$ is the number of half-cycles to failure, and α and Θ_f are material constants (further detail is available in [13]). The effect of strain history and varying strain amplitudes can be included using the linear cumulative damage hypothesis known as Miner's rule [39]. Based on Miner's rule, applying n_1 half cycles with a strain amplitude ε_1 and corresponding fatigue life of $2N_{f1}$, is equivalent to consuming $n_1/2N_{f1}$ of the fatigue resistance.

The same assumption applies to any subsequent block of load cycles. Accordingly, the cumulative low-cycle fatigue damage can be estimated. Further details and derivation of the equations are available in [13]. Brown and Kunnath [37] calibrated the material constants α and Θ_f using data from low-cycle fatigue tests of uncorroded bars subjected to constant amplitude cyclic loading. The reported calibrated values of Θ_f and α are 0.12 and 0.44 respectively. A schematic of the cyclic degradation model for reinforcing bars that is used in this research is shown in Fig. 11.

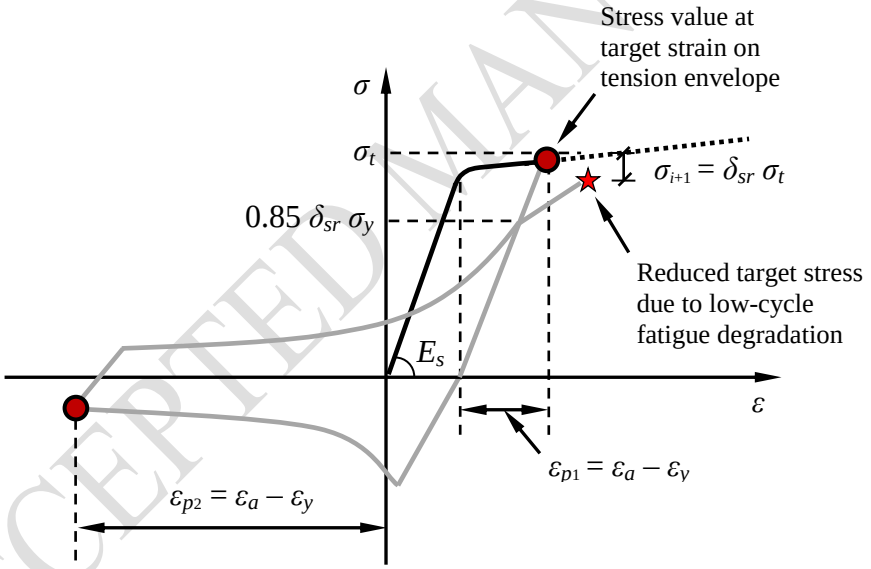

Fig. 11 Low-cycle high amplitude fatigue degradation model of reinforcing bars

3 Modelling the influence of corrosion on nonlinear response of corrosion damaged reinforcing bars

3.1 Impact of corrosion damage on tension envelope (state TE)

The effect of corrosion damage on the mechanical properties of reinforcing bars has been investigated by several researchers [40-44]. Most have come to the conclusion that non-uniform pitting corrosion affects the average stress-strain response of corroded bars. More

recently, Apostolopoulos *et al.* [45] investigated the influence of pitting depth on the mechanical properties of corroded bars. They concluded that stress concentrations at the pitting locations result in a significant degradation in mechanical properties of corroded bars. Therefore, in the modelling of the cyclic behaviour of corroded bars consideration needs to be given to the modified tension envelope. Du *et al.* [41, 42] provides a detailed description of the effect of corrosion damage on residual capacity and ductility of corroded bars in tension. In this section the proposed methodology suggested by [41, 42] is adopted to account for the influence of pitting corrosion on the stress-strain behaviour of reinforcing bars in tension. They concluded that the effect of corrosion on the tension stress-strain curve of corroded bars can be modelled by employing a pseudo stress-strain curve with modified yield stress as shown in Fig. 12.

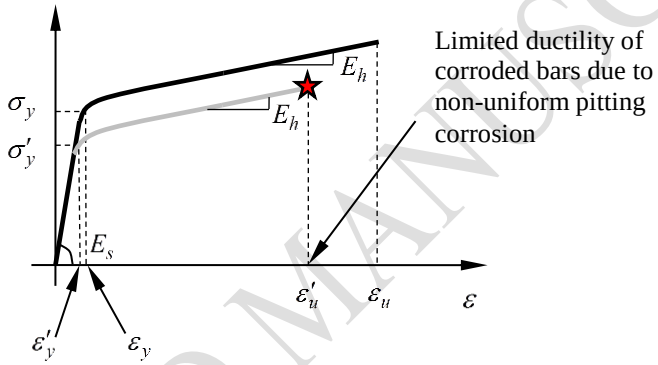

Fig. 12 Modified tension envelope curve of corroded bars

The modified yield stress and strain of the corroded reinforcement can be calculated using Eqs. (19) and (20) below:

$$\sigma'_y = \sigma_y(1-\beta_s\,\psi) \tag{19}$$

$$\varepsilon'_u = \varepsilon_u(1-\beta_e\,\psi) \tag{20}$$

where, σ'_y is the yield stress of a corroded bar in tension, σ_y is the corresponding yield stress of the uncorroded bar and ψ is the percentage mass loss due to corrosion. The value of β_s is 0.005 and β_e is 0.05 as reported by [41, 42] The β_s and β_e are empirical coefficients known as *pitting coefficients* that account for the influence of on premature fracture and reduced capacity of corroded reinforcing bars.

The influence of corrosion on cross section loss is taken into account by considering an average reduced cross section area assuming a uniform mass loss using Eq. (21) below:

$$D' = \frac{D_0}{10}\sqrt{100 - \psi} \tag{21}$$

where, D' is the average reduced diameter of corroded reinforcement, D_0 is the initial diameter of uncorroded reinforcement and ψ is the percentage mass loss due to corrosion.

3.2 Impact of corrosion damage on post-yield buckling response (state CE)

The influence of corrosion on the inelastic buckling behaviour of corroded reinforcing bars has been investigated by Kashani *et al.* experimentally [26] and computationally [28]. Computational studies show that there are three main parameters that influence the buckling behaviour of corroded bars. These parameters are (a) irregular loss of cross section area and second moment of area along the length of the bar, (b) shifting of the centroid of the bar cross section along of the bar that results in load eccentricity and (c) cross sectional shape of the bar which is very important inelastic buckling. These parameters cause stress concentrations and exacerbate imperfections, and, as a result, reduce the buckling capacity.

Due to the complexity of the problem and the random nature of corrosion, it is difficult to develop a mechanistic model equation defining the impact of corrosion on the parameters that determine buckling response. Here, the empirical equations developed by Kashani *et al*. [26] are used to modify the compression response curve for corroded reinforcement. The proposed modifications to the post-yield buckling response of corroded bars are shown in Fig. 13.The proposed model shown in Fig. 13 is based on the observed experimental results reported in [26].

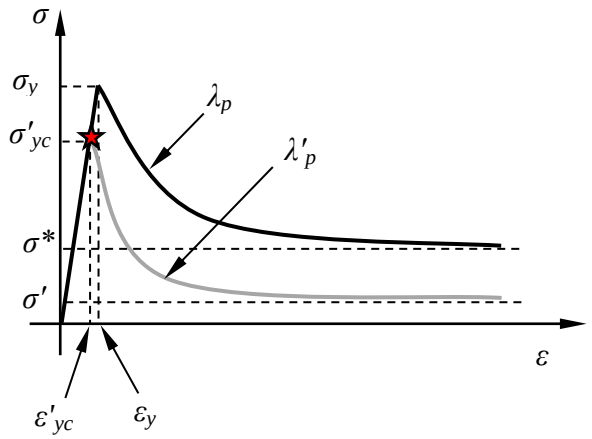

Fig. 13 Modified post-yield buckling envelope curve of corroded bars

The effect of corrosion on compressive yield strength (σ'_{yc}) is defined using the empirical Eq. (22), which is calibrated based on the observed experimental results:

$$\sigma'_{yc} = \begin{cases} \sigma_y\left(1-0.005\,\psi\right) & \text{for } L/D \le 6 \\ \sigma_y\left(1-0.0065\,\psi\right) & \text{for } 6 < L/D < 10 \\ \sigma_y\left(1-0.0125\,\psi\right) & \text{for } L/D \ge 10 \end{cases} \tag{22}$$

For uncorroded reinforcement, the buckling response model is a function of the non-dimensional slenderness ratio, λ_p, and the minimum stress limit asymptotic σ^* per Eqs. (3)-(6). Therefore, the yield stress and diameter of a corroded bar in Eqs. (3) to (6) can be modified using Eqs. (21) and (22) to account for the impact of corrosion on buckling parameters.

Fig. 14 (a-d) shows the buckling response predicted by the proposed model, as defined using modified Eqs. 3-6 with λ'_p and σ'_{yc}, and experimental data for corroded bars with different percentages mass loss and slenderness ratios. The data in Fig. 14 show the proposed model is in a good agreement with the experimental results.

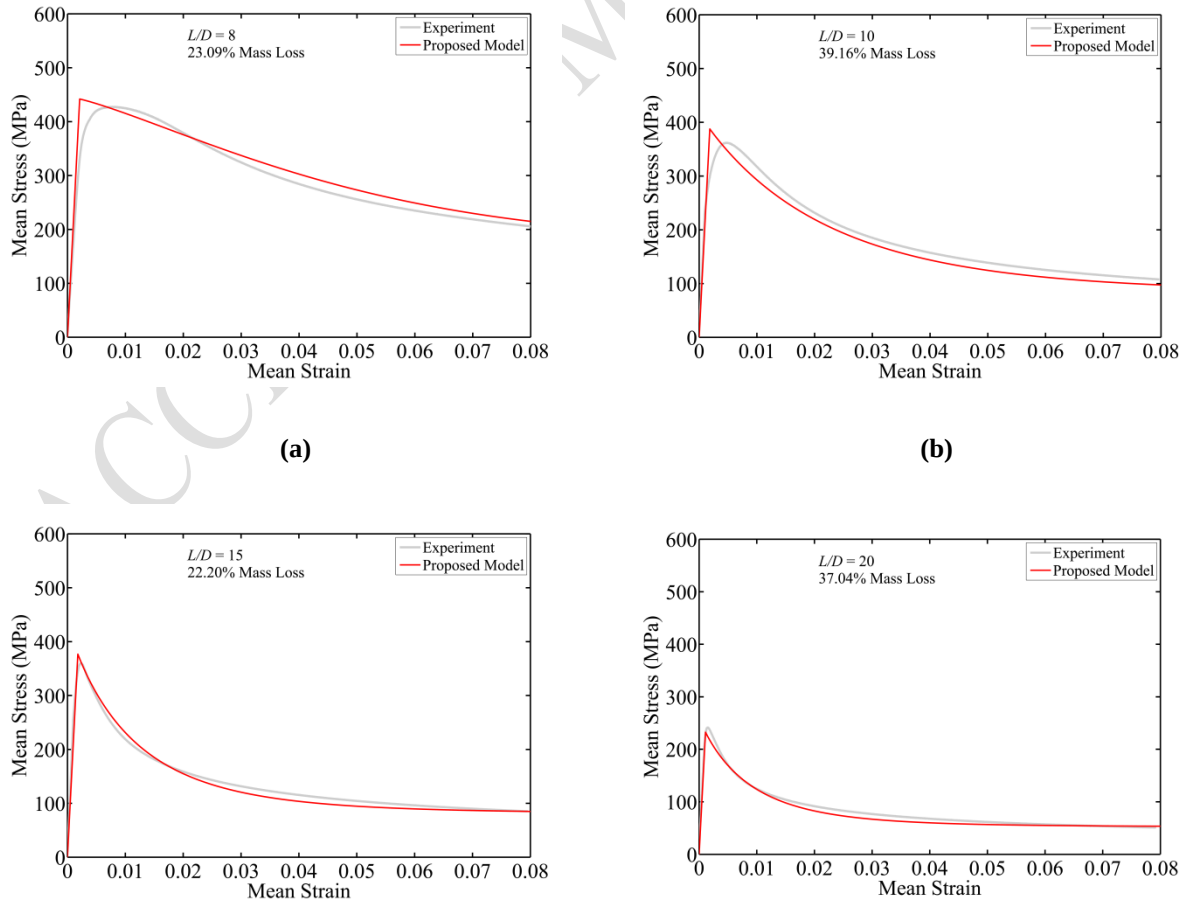

(c) **(d)**

Fig. 14 Verification of the proposed model with observed experimental response of corroded bars: (a) *L/D* = 8 (b) *L/D* = 10 (c) *L/D* = 15 (d) *L/D* = 20

3.3 Modelling the influence of corrosion on low-cycle fatigue degradation (state FATDEG)

Kashani et al. [23] investigated low-cycle fatigue behaviour for corroded bars using data from tests in which bars were subjected to cyclic loading with increasing strain amplitude. They found that corrosion doesn't influence the material constant Θ_f. However, corrosion does change the material constant α. The relationship between percentage mass loss and the material constant α, based on the reported experimental data, is shown in Eq. (23) below:

$$\frac{\alpha_{corr}}{\alpha} = 1 + 0.004\psi \tag{23}$$

where, α_{corr} is the material constant of corroded bars. Accordingly the value of α in fatigue life model can be replaced with α_{corr} to account for the influence of non-uniform pitting on fatigue life.

4 Model verification

4.1 Nonlinear cyclic response of uncorroded reinforcing bars

Fig. 15 shows cyclic response histories for uncorroded reinforcing bars as determined from laboratory testing [23] and as simulated using the proposed model. The bars have relatively high slenderness ratios and exhibit severe buckling under compressive loading as well as strength deterioration due to low-cycle high-amplitude fatigue. The error in total hysteretic energy dissipation is used to quantify the accuracy of the model (Eq. (24)).

$$\Omega = \frac{\left| E_{\text{model}} - E_{\text{exp}} \right|}{E_{\text{exp}}} \tag{24}$$

Ω is the error in the model, E_{model} is the total hysteretic dissipated energy in the model and E_{exp} is the total hysteretic dissipated energy in experiment. It was found the error in Fig. 15 (a) and (b) was 0.7% and 0.6% respectively.

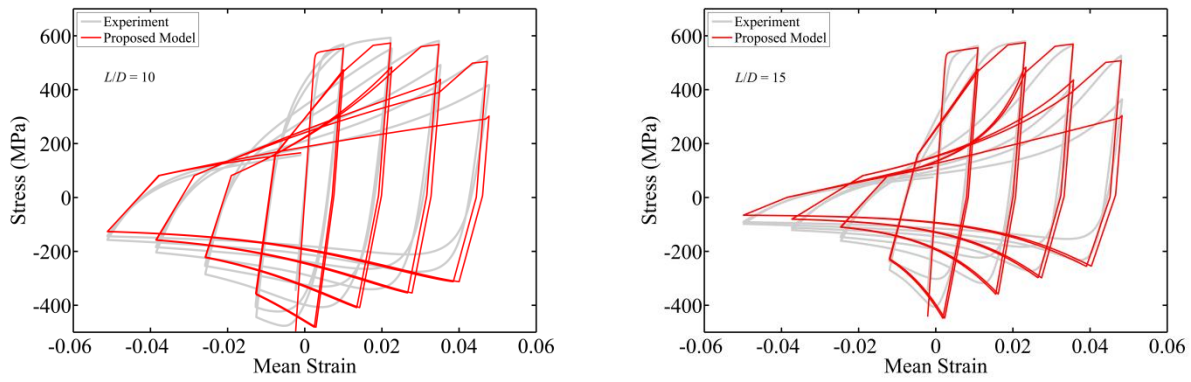

(a) **(b)**

Fig. 15 Comparison of the proposed model with physical testing of uncorroded reinforcement: a) *L/D* = 10 and b) *L/D* = 15

4.2 Nonlinear cyclic response of corroded reinforcing bars

Fig. 16 (a-d) shows cyclic response histories for four corroded reinforcing bars as determined from laboratory testing [23] and as simulated using the proposed model. The bars have relatively high slenderness ratios and exhibit buckling under compressive loading as well as strength deterioration due to low-cycle high-amplitude fatigue. The bars have moderate mass-loss due to corrosion with mass-loss ratios ranging from 10% to 27%.

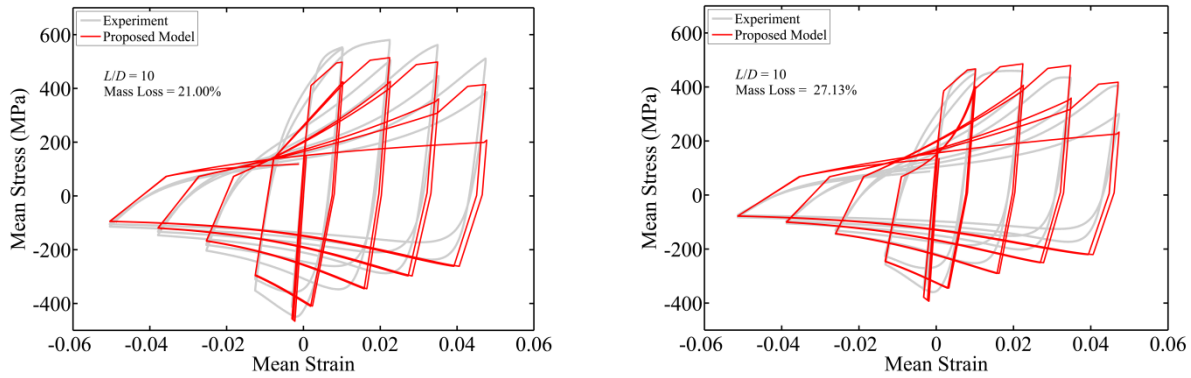

(a) **(b)**

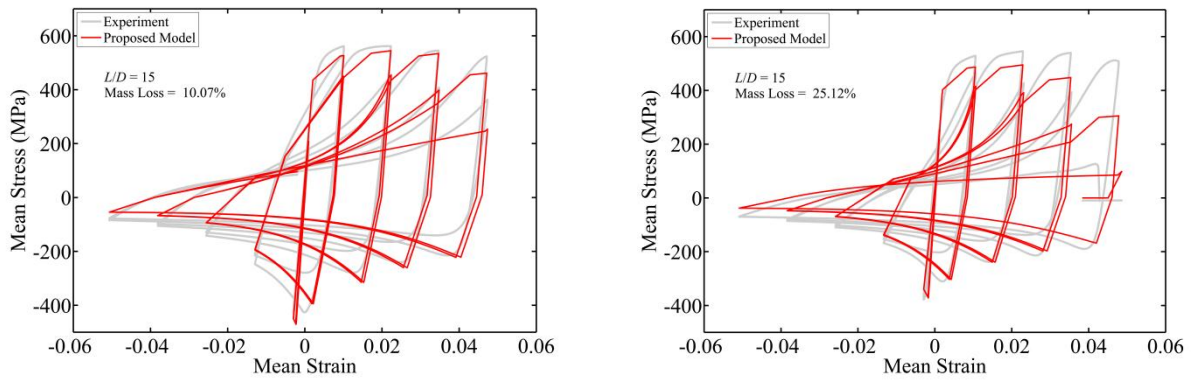

(c) **(d)**

Fig. 16 Comparison of the proposed model with physical testing of corroded reinforcement: a) *L*/*D* = 10 and 21% mass loss, b) *L*/*D* = 10 and 27.13% mass loss, c) *L*/*D* = 15 and 10.07% mass loss and d) *L*/*D* = 15 and 25.12% mass loss

As with the uncorroded bars, experimental and simulation results for corroded bars were compared on the basis of the response envelop for tension, the response envelope for compression, and hysteretic energy dissipation. It shows that the error in hysteretic energy dissipation in the model is varied from 5% to about 15%. The complete list of calculated error of the entire dataset is tabulated in the Table 2 and 3. It should be noted that the difference between simulated and observed dissipated energy was found to be higher for bars with severe localised pitting corrosion.

This could be expected given that the cyclic buckling response of corroded reinforcement is controlled by the section with the minimum area, minimum second moment of area, and maximum eccentricity. Fig. 17 (a) shows the proportionality of the dissipated energy in the model and experiment for the entire experimental dataset. Kashani *et al*. [27] provide data characterising the variation in geometric properties for corroded reinforcement; future research will seek to use these data to develop *effective* mass loss ratios that capture the potential for localised pitting corrosion to result in degraded response.

Fig. 17 (b) shows the mean (μ) and standard deviation (σ) of the ratio of dissipated energy in the model to the dissipated energy in the experimental dataset. The calculated μ and σ for the entire dataset are 0.9774 and 0.0805 respectively. The μ and σ of the error in dissipated energy in the model together with the ratio of the calculated and experimental dissipated energy for each group of experimental data are also shown in Table 2 and 3.

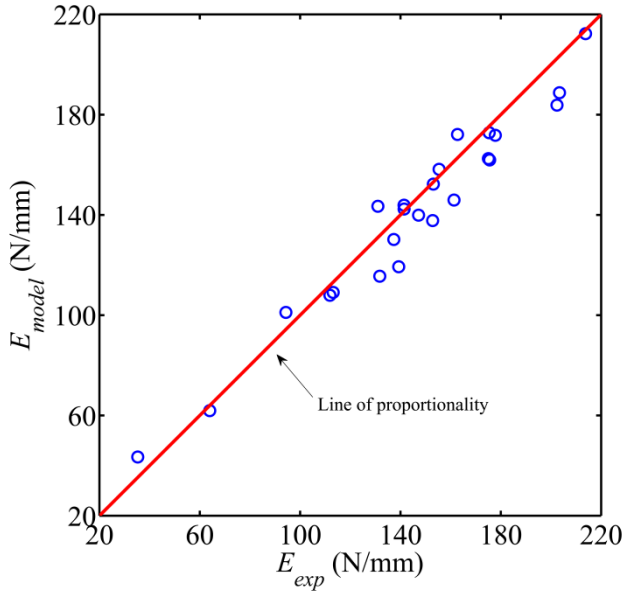

(a)

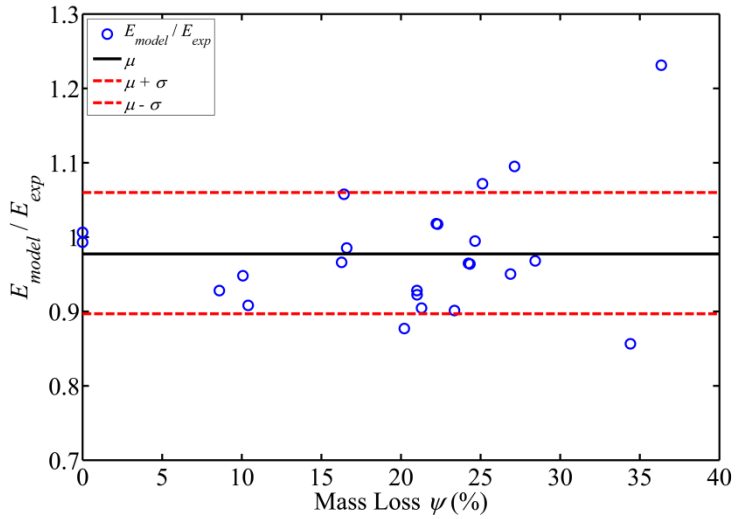

(b)

Fig. 17 Comparison of the total hysteretic energy dissipation ion the model and experimental data set: (a) Proportionality of dissipated energy in the model and experiment (b) mean and standard deviation

Table 2 Model Error for group of bars with L/D = 10

Mass Loss (%)	E_{exp} (N/mm)	E_{model} (N/mm)	E_{model} / E_{exp}	$\Omega = \lvert E_{model} - E_{exp} \rvert / E_{exp}$
0.00	213.79	212.32	0.993	0.007
8.59	203.39	188.76	0.928	0.072
10.40	202.38	183.81	0.908	0.092
16.27	177.81	171.78	0.966	0.034
16.42	162.73	172.11	1.058	0.058
16.59	175.37	172.79	0.985	0.015
21.00	175.05	162.47	0.928	0.072
21.01	175.55	161.93	0.922	0.078
21.29	161.34	145.94	0.905	0.095
22.22	155.39	158.20	1.018	0.018
22.30	141.42	143.88	1.017	0.017
23.36	152.83	137.75	0.901	0.099
24.65	153.11	152.29	0.995	0.005
26.88	147.21	139.90	0.950	0.050
27.13	131.00	143.45	1.095	0.095
34.41	139.31	119.33	0.857	0.143
36.31	4.16	7.73	1.859	0.859
Mean (μ)			0.9642	0.0593
Std. deviation (σ)			0.0635	0.0406

Table 3 Model Error for group of bars with L/D = 15

Mass Loss (%)	E_{exp} (N/mm)	E_{model} (N/mm)	E_{model} / E_{exp}	$\Omega = \lvert E_{model} - E_{exp} \rvert / E_{exp}$
0.00	141.44	142.34	1.006	0.006
10.07	137.34	130.21	0.948	0.052
20.21	131.75	115.55	0.877	0.123
24.24	111.88	107.94	0.965	0.035
24.33	113.18	109.09	0.964	0.036
25.12	94.34	101.11	1.072	0.072
28.43	63.97	61.92	0.968	0.032
36.35	35.27	43.42	1.231	0.231
Mean (μ)			0.9812	0.1408
Std. deviation (σ)			0.1068	0.0726

For further validation, the model is compared against a set of experimental data that were not included in the model calibration process. Fig. 18 (a) shows the comparison of the proposed model with a corroded bar with L/D = 15 and 19.93% mass loss under monotonic loading and Fig. 18 (b) shows the comparison of the proposed model with a corroded bar with L/D = 10 and 15.48% mass loss under cyclic loading.

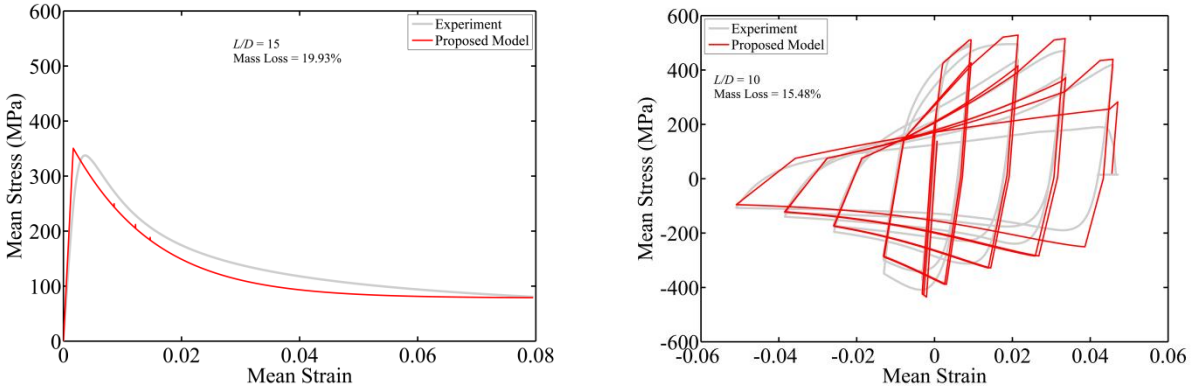

(a) **(b)**

Fig. 18 Comparison of the proposed model and experimental tests that were not included in model calibration process: (a) L/D = 15 and 19.93% mass and (b) L/D = 10 and 15.48% mass loss

With reference to Figs. 15-18, it is evident that the proposed model can accurately predict the nonlinear cyclic response of uncorroded and corroded reinforcing bars with the effect of inelastic buckling and low-cycle high-amplitude fatigue degradation. The proposed model is simple and can be readily implemented in any finite element programme for nonlinear analysis of RC structures subject to earthquake loading.

5 Implementation and application of the proposed model

To facilitate community use of the model presented in this paper, it has been implemented in OpenSees, an open-source software framework for simulating the earthquake response of structures that was originally developed by researchers at the Pacific Earthquake Engineering Research Centre (PEER) [3]. An executable version of OpenSees that includes this model is available at http://opensees.berkeley.edu. OpenSees is an object-oriented software framework written primarily in C^{++}. Implementation of the cyclic buckling model comprised creation of a new *UniaxialMaterial*, *CorrodedReinforcingSteel*. Specifically a *.cpp file was created that defines the response logic described in this paper and a *.h file was created that defines all the history variables to be used in the nonlinear solution procedure.

Fig. 19 shows a simplified version of the OpenSees abstract class structure including the new *CorrodedReinforcingSteel* class. In Fig. 19, the *Domain* maintains the information necessary to describe and represent the state of the model throughout the analysis. The *Domain* class controls multiple subclasses including the Material subclass, and the *Material* class controls multiple subclasses including the *UniaxialMaterial* subclass.

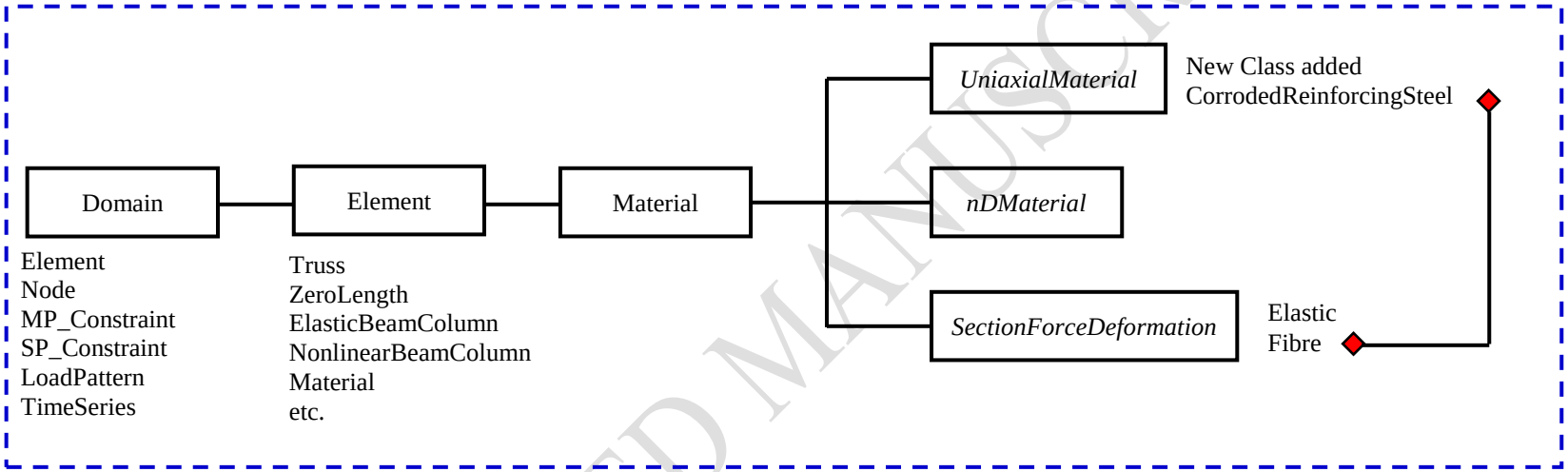

Fig. 19 Partial OpenSees abstract classes map representing the new implemented class [46-48]

Further details of implementation procedure are available in [49]. To demonstrate the impact of buckling, low-cycle fatigue and corrosion damage on response, OpenSees and the newly implemented *CorrodedReinforcingSteel* class were used to simulate the behaviour of a reinforced concrete section subjected to zero axial load and a cyclic curvature history. Fig 20a shows the section considered and provides relevant material properties. The section consists of 8 number 16 mm diameter reinforcing bars with 500MPa yield strength. The section was discretised into 25 × 25 concrete fibres and eight steel fibres.

The unconfined concrete is considered for cover concrete. Confined concrete is considered for core concrete with a nominal confinement factor K = 1.3 using *Concrete02 UniaxialMaterial* available in OpenSees. This material model assumes stress-strain response in compression is parabolic to maximum strength and bilinear in the post-peak regime. The residual compressive strength is 0.1 K f'_c at strain demands in excess of first hoop reinforcement fracture. The stress-strain response in tension is assumed to be linear to maximum strength and linear post-peak with zero tensile strength for strain demands in excess of 0.001. Steel response was modelling using the *CorrodedReinforcingSteel UniaxialMaterials* (Fig 20b).

Analyses were performed for two L/D ratios and for the cases of no corrosion and mass loss due to corrosion. The L/D ratio employed in the model may be related to the s/d ratio for the section, where s is spacing of transverse reinforcement and d is the diameter of longitudinal reinforcement using the model proposed by Dhakal and Maekawa [20]. Analyses were done also using the *Steel02* model available in OpenSees; this model assumes a bilinear response envelope, employs Menegotto-Pinto curves [29] to describe unload-reload response and does not simulated buckling or the impact of low-cycle fatigue (Fig 20c).

It should be noted that corrosion damage to RC components affects concrete as well as steel response; corrosion result in cracking of cover concrete, reducing the passive confinement pressure of core concrete, premature fracture of horizontal tie reinforcement and reduced bond strength. However, to demonstrate the proposed model and the impact of cyclic buckling on corroded and uncorroded section response, these aspects of behaviour were not considered in the in the analyses.

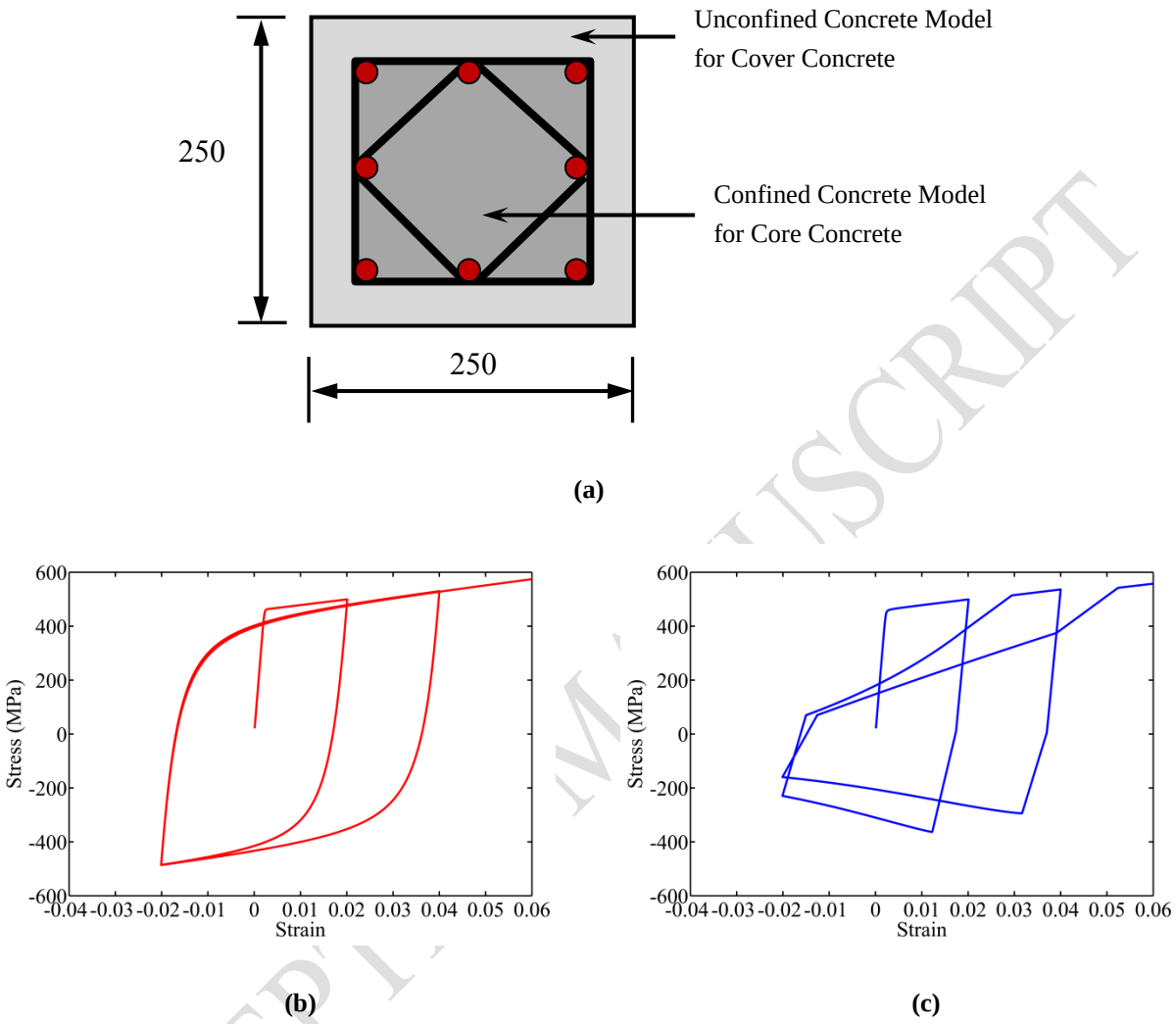

Fig. 20 RC section and material data: (a) section geometry (b) *Steel02* (c) *CorrodedReinforcingSteel*

Fig. 21 (a) shows simulated moment-curvature response for the section for the different steel models and L/D ratios. Fig. 21 (b) shows simulation results generated using the proposed model with L/D = 15 and varying mass loss ratios. As it is shown in Fig. 21 the inelastic buckling of reinforcing bars has a significant influence on the inelastic section response.

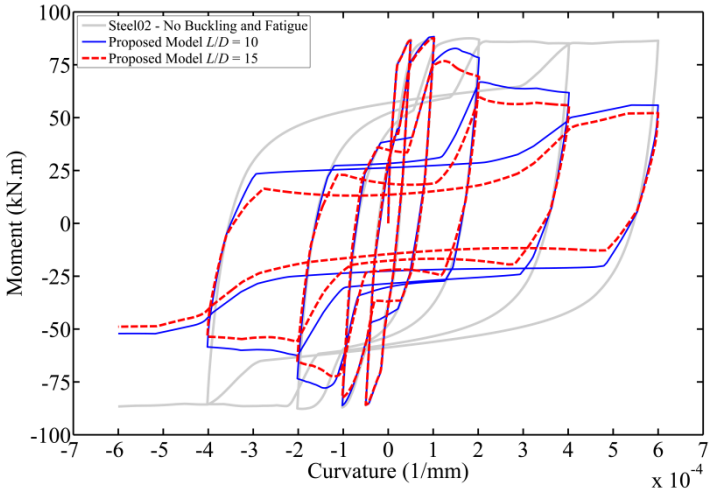

(a)

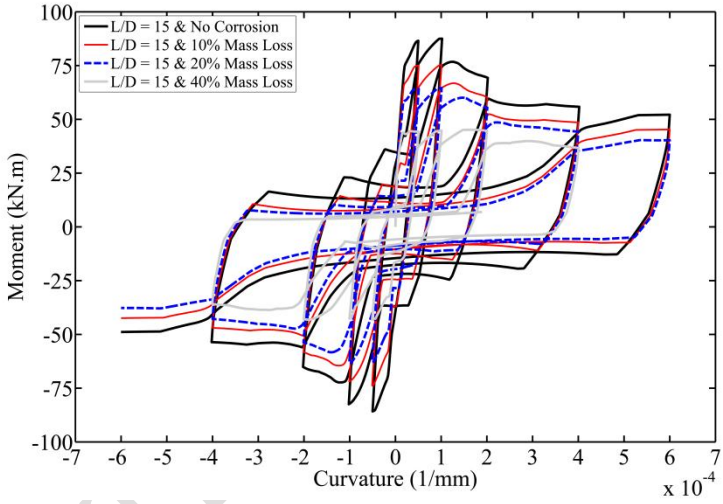

(b)

Fig. 21 Moment-curvature analysis of RC section

The comparison between the moment-curvature response of the hypothetical RC section using *Steel02* and the new *Corrodedreinforcingsteel* shows that the inelastic behaviour of RC sections is mainly govern by the inelastic behaviour of reinforcing steel. This is a very important observation as it greatly influences the energy dissipation capacity of RC structures during large earthquakes. Moreover, it is much more critical for those structures located in high seismicity regions as corrosion significantly reduces the energy dissipation capacity of corroded structures. Furthermore, the combined effect of inelastic buckling and cyclic degradation due to low-cycle fatigue has a significant contribution if premature collapse of corroded RC structures. This has also been observed in experimental studies by other researchers [24, 25]. In recent years other researchers developed new fractional derivative

models for concrete structures and diffusion equations that predict the diffusion of chloride ions in concrete and corrosion initiation time [50-52]. The proposed model in this paper combined with [50-52] provide an opportunity to other researchers to investigate the impact of inelastic buckling, low-cycle fatigue degradation and corrosion on seismic vulnerability and risk assessment of RC structures.

6 Conclusions

A new phenomenological model is presented that simulates the inelastic buckling response of uncorroded and corroded reinforcing steel subjected to cyclic loading. The model was developed using data from laboratory testing and from nonlinear finite element analysis of bare reinforcing bars subjected to monotonic and cyclic loading. The model simulates inelastic buckling, the impact of low-cycle high-amplitude fatigue degradation on the nonlinear response, and the impact of mass loss due to corrosion. Response is defined on the basis of *i*) steel material properties, *ii*) nominal reinforcement area, *iii*) the reinforcement slenderness ratio, which may be computed from the bar diameter and spacing of horizontal reinforcement using the model proposed by Dhakal and Maekawa [20], and *iv*) mass loss due to corrosion. To facilitate use of the model, it has been implemented in OpenSees, an open-source software framework for nonlinear finite element analysis of structures. The primary observations and outcomes of this research are as follows:

1. The proposed model in most cases can accurately simulate the inelastic buckling and low-cycle fatigue degradation of corroded bars. However, severe localised pitting corrosion might result in an inaccurate simulation. Previous research [28] showed that the stress-strain behaviour of these bars is mainly governed by the minimum section. Given the complexity and highly uncertainty associated with localisation of corrosion, this problem should be solved probabilistically. This is an area for further research.

2. The proposed model was developed using data from laboratory tests and numerical simulation of bare reinforcing bars. Further research is required to verify that use of this model enables accurate simulation of the cyclic response of reinforced concrete components.

3. Experimental and simulation data show that for reinforcing bars with $L/D \geq 8$ inelastic buckling results in a pinched hysteretic response while bars with $L/D < 8$ exhibit a hysteretic response that is similar to steel material response (*steel02*). The proposed

model simulates a pinched hysteretic response (combined material and geometrical nonlinearity) and, thus, is appropriate for use for reinforcement with $L/D \geq 8$. For reinforcement with $L/D < 8$, existing models (*steel02*) that do not simulate buckling are appropriate.

4. The proposed model presented in this paper combines the material nonlinearity and geometrical nonlinearity due to buckling with low-cycle fatigue degradation in to a single material model. Therefore, it is currently the most advanced uniaxial material model which is purposely developed for reinforcing bars with and without corrosion damage. This has successfully been implemented in the OpenSees and is readily available to be used by the earthquake engineering community.

7 Acknowledgements

The experimental work is funded by the Earthquake Engineering Research Centre (EERC) of the University of Bristol. The computational part of this research is conducted in collaboration with the University of Washington while the first author was on sabbatical leave in the USA. The funding provided by the World Wide University Network through Research Mobility Programme to the first author is much appreciated. Any findings, opinions and recommendations provided in this paper are only based on the author's view.

Reference

[1] E. Spacone, F. C. Filippou and F. F. Taucer, Fibre beam-column model for non-linear analysis of R/C frames: part I: formulation, Earthq Eng Struct D, 25 (1996) 711-725.

[2] E. Spacone, F. C. Filippou and F. F. Taucer, Fibre beam-column model for non-linear analysis of R/C frames: part II: applications, Earthq Eng Struct D, 25 (1996) 727-742.

[3] OpenSees, the Open System for Earthquake Engineering Simulation, Pacific Earthquake Engineering Research Centre (2012), University of California, Berkeley.

[4] SeismoStruct v5.2.2; Seismosoft Earthquake Engineering Software Solutions (2011).

[5] SAP2000 Structural analysis and design software, Computers and Structures Inc. (2013).

[6] M. P. Berry and M. O. Eberhard. Performance modeling strategies for modern reinforced concrete bridge columns. 67 (11) (2006).

[7] M. P. Berry, D. E. Lehman and L. N. Lowes. Lumped-plasticity models for performance simulation of bridge columns, ACI Strut. J. 105 (3) (2008) 270-279.

[8] J. S. Pugh. Numerical Simulation of Walls and Seismic Design Recommendations for Walled Buildings. PhD Thesis, University of Washington 2013.

[9] G. Monti and C. Nuti, Nonlinear cyclic behavior of reinforcing bars including buckling, J Struct Eng, 118 (12) (1992) 3268–3284.

[10] M. E. Rodriguez, J. C. Botero and J. Villa, Cyclic stress-strain behavior of reinforcing steel including the effect of buckling, J Struct Eng, 125 (6) (1999) 605–612.

[11] A. Gomes and J. Appleton, Nonlinear cyclic stress-strain relationship of reinforcing bars including buckling, Engineering Structures, 19 (1997) 822–826.

[12] S. Bae, A. Mieses and O. Bayrak, Inelastic buckling of reinforcing bars, J Struct Eng, 131 (2) (2005) 314–321.

[13] S. K. Kunnath, Y. Heo and J.F Mohle, Nonlinear uniaxial material model for reinforcing steel bars, J Struct Eng, 135 (4) (2009) 335–343.

[14] L. L. Dodd and J. I. Restrepo-Posada, Model for predicting cyclic behavior of reinforcing steel, J Struct Eng, 121 (3) (1995) 433–445.

[15] T. A. Balan, F. C. Filippou and E.P. Popov, Hysteretic model of ordinary and high-strength reinforcing steel, J Struct Eng, 124 (3) (1998) 288–97.

[16] M. S. Hoehler and J. F. Stanton, Simple phenomenological model for reinforcing steel under arbitrary load, J Struct Eng, 132 (7) (2006) 1061-1069.

[17] G.A. Chang and J.B. Mander, Seismic energy based fatigue damage analysis of bridge columns: Part I – Evaluation of seismic capacity. Technical report NCEER-94-0006, 1994.

[18] R. Dhakal and K. Maekawa, Modeling for postyield buckling of reinforcement, J Struct Eng, 128 (9) (2002) 1139–1147.

[19] R. Dhakal and K. Maekawa, Path-dependent cyclic stress-strain relationship of reinforcing bar including buckling, Eng Struct, 24 (2002) 1139–1147.

[20] R. P. Dhakal and K. Maekawa, Reinforcement stability and fracture of cover concrete in reinforced concrete members, J Struct Eng, 128 (10) (2002) 1253–1262.

[21] H. Nakamura, and T. Higai, Modeling nonlinear cyclic behavior of reinforcing bars, ACI SP 205-14, 205 (2002) 273-292.

[22] A. Prota, F. Cicco and E. Cosenza, Cyclic behavior of smooth steel reinforcing bars: experimental analysis and modeling issues, J Earthq Eng, 13 (2009) 500-519.

[23] M. M. Kashani, A. J. Crewe, N. A. Alexander, Nonlinear cyclic response of corrosion-damaged reinforcing bar with the effect of buckling, Constr Build Mater 41 (2013) 388-400.

[24] Y. Ou, L. Tsai, H. Chen, Cyclic performance of large-scale corroded reinforced concrete beams, Earthq Eng Struct D 41 (2011) 592-603.

[25] Y. Ma, Y. Che, J. Gong, Behavior of corrosion damaged circular reinforced concrete columns under cyclic loading, Constr Build Mater 29 (2012) 548–556.

[26] M. M. Kashani, A. J. Crewe, N. A. Alexander, Nonlinear stress-strain behaviour of corrosion-damaged reinforcing bars including inelastic buckling, Eng Struct 48 (2013) 417–429.

[27] M. M. Kashani, A. J. Crewe, N. A. Alexander, Use of a 3D optical measurement technique for stochastic corrosion pattern analysis of reinforcing bars subjected to accelerated corrosion, Corros Sci 73 (2013) 208–221.

[28] M. M. Kashani, L.N. Lowes, A. J. Crewe, N. A. Alexander, Finite element investigation of the influence of corrosion pattern on inelastic buckling and cyclic response of corroded reinforcing bars, Eng Struct, 75 (2014) 113–125.

[29] M. Menegotto and P.E. Pinto, Method of analysis of cyclically loaded RC plane frames including changes in geometry and nonelastic behavior of elements under normal force and bending. Preliminary Report IABSE, Zurich, 13 (1973) 15–22.

[30] S. T. Mau, M. El-Mabsout, Inelastic buckling of reinforcing bars, J of Eng Mech, 115 (1) (1989) 1-17.

[31] C. D. Hill, G. E. Blandford and S. T. Wang, Post-buckling analysis of steel space trusses, J Struct Eng, 115 (4) (1989) 900-919.

[32] H. T. Thai and S. E. Kim, Nonlinear inelastic time-history analysis of truss structures, J of Constructional Steel Res, 67 (2011) 1966-1972.

[33] MTLAB R2012b, The MathWorks lnc, www.mathworks.com, 1994-2012

[34] T. Higai, H. Nakamura and S. Saito, Fatigue failure criterion for deformed bars subjected to large deformation reversals, ACI SP 237-4, 237 (2006) 37-54.

[35] R. A. Hawileh, J. A. Abdalla, F. Oudah and K. Abdelrahman, Low-cycle fatigue life behaviour of BS 460B and BS B500B steel reinforcing bars, Fatigue Fract Eng M, 33 (2010) 397-407.

[36] J. B. Mander, F. D. Panthaki and A. Kasalanat, Low-cycle fatigue behavior of reinforcing steel, J Mater Civil Eng, 6 (4) (1994) 453–468.

[37] J. Brown and S.K. Kunnath, Low-cycle Fatigue failure of reinforcing steel bars, ACI Mater J, 101(6) (2004) 457–466.

[38] S. S. Manson, Fatigue: A complex subject-Some simple approximations, Exp Mech, 5 (7) (1965) 193–226.

[39] M. A. Miner, Cumulative damage in fatigue, J Appl Mech, 12 (1945) A159–A164.

[40] A. A. Almusallam, Effect of degree of corrosion on the properties of reinforcing steel bars, Constr Build Mater, 15 (2001) 361-368.

[41] Y. G. Du, L.A. Clark and A.H.C. Chan, Residual capacity of corroded reinforcing bars, Magazine of Concrete Research, 57 (3) (2005) 135–147.

[42] Y. G. Du, L.A. Clark and A.H.C. Chan, Effect of corrosion on ductility of reinforcing bars, Magazine of Concrete Research, 57 (7) (2005) 407–419.

[43] J. Cairns, G.A. Plizzari, Y.g. Du, D.W. Law and F. Chiara, Mechanical properties of corrosion-damaged reinforcement, ACI Mater J, 102 (4) (2005) 256–264.

[44] C. A. Apostolopoulos, M.P. Papadopoulos and S.G. Pantelakis, Tensile behavior of corroded reinforcing steel bars BSt 500s, Constr Build Mater, 20 (2006) 782–789.

[45] C.A. Apostolopoulos, S. Demis and V.G. Papadakis, Chloride-induced corrosion of steel reinforcement-Mechanical performance and pit depth analysis. Constr Build Mater, 38 (2013) 139-146.

[46] G. C. Archer, G. Fenves, C. Thewalt, A new object-oriented finite element analysis program, Comput Struct, 70 (1999) 63-75.

[47] G. C. Archer, Object-Oriented Finite Element Analysis, PhD Thesis, University of California, Berkeley, 1996.

[48] F. T. McKenna, Object-oriented finite element programming: frameworks for analysis, algorithms and parallel computing, PhD Thesis, University of California, Berkeley, 1997.

[49] M. M. Kashani, Seismic Performance of Corroded RC Bridge Piers: Development of a Multi-Mechanical Nonlinear Fibre Beam-Column Model, PhD Thesis, University of Bristol, 2014.

[50] W. Chen, J.J. Zhang, J.Y. Zhang, A variable-order time-fractional derivative model for chloride ion sub-diffusion in concrete structures, Fractional Calculus and Applied Analysis, 16 (1) (2013) 76-92.

[51] Z. Fu, W. Chen, H.T. Yang. Boundary particle method for Laplace transformed time fractional diffusion equations, Journal of Computational Physics, 235(15) (2013) 52-66.

[52] H. G. Sun, W. Chen, Y. Q Chen, Variable-order fractional differential operators in anomalous diffusion modeling, Physica A: Statistical Mechanics and its Applications, 388(21) (2009) 4586-4592.